Editors' Suggestion | Featured in Physics

Sea Ice Aging by Diffusion-Driven Desalination

Yihong Du,[1] Feng Wang,[1,*] Enrico Calzavarini,[2] and Chao Sun[1,3]
[1]New Cornerstone Science Laboratory, Center for Combustion Energy, Key Laboratory for Thermal Science and Power Engineering of MoE, Department of Energy and Power Engineering, Tsinghua University, Beijing 100084, China
[2]Université Lille, Unité de Mécanique de Lille - J. Boussinesq (UML) ULR 7512, F-59000 Lille, France
[3]Department of Engineering Mechanics, School of Aerospace Engineering, Tsinghua University, Beijing 100084, China

(Received 27 February 2025; revised 25 May 2025; accepted 30 June 2025; published 5 September 2025)

Sea ice is a key component of Earth's climate system, making its aging process an essential focus of current research. The age of sea ice is closely linked to its thermal and mechanical properties, which govern its interactions with the surrounding environment. In this study, we combine experimental techniques and modeling to explore the full dynamical process of mushy ice growth and spontaneous aging in saline water, within a natural convective flow system. We show that the aging of newly formed mushy ice in the present system, characterized by a gradual long-term reduction in porosity, is controlled by diffusion-driven desalination. Moreover, we observe that the system eventually transits into a dense freshwater ice layer adjacent to a well-mixed saline water region. The shape of the ice layer in this asymptotic state is well captured by numerical simulations of nonporous ice. Our findings improve the understanding of the complex physics governing phase changes in aqueous systems and provide a framework for studying sea ice aging in laboratory settings, with implications spanning diverse natural and industrial applications.

DOI: 10.1103/mct1-6hbw

In the cryosphere, sea ice evolves through distinct stages: First-year ice becomes second-year ice and eventually multiyear ice [1]. The stage of ice development (also called the ice age) directly influences its thermal and mechanical properties [2]. These properties play a critical role in how sea ice responds to environmental forces [3–5]. Changes in the spatial distribution of sea ice age [6,7] have important implications for the ice's melting rate, areal extent, and surface albedo, which can significantly affect a variety of climatic [8,9], environmental [10], and ecological [11,12] processes.

One distinct difference between first-year sea ice and older sea ice is their porosity. Porosity is positively correlated with the salt content of the ice [2]. Previous studies have shown that sea ice undergoes significant desalination as it ages [13–15]. Mushy layer theories have been proposed to describe the salt and heat transport as well as to estimate effective thermal properties [13,16–18], which are applicable to mushy sea ice. However, the dynamic aging process of mushy ice and its relationship with ice desalination still require further investigation, particularly through the integration of models and observations.

Laboratory studies have proven to be valuable for understanding the coupled physics of phase change and fluid flows in various scenarios [1,19–28]. Many studies have explored the effects of brine convection in mushy ice on its structure and dynamics [29–35]. These studies focused primarily on the initial growth of ice and did not examine the long-term aging process. More recently, laboratory experiments and simulations have revealed the rich dynamics of ice melting in salty water under various conditions [36–38]. However, in these studies, a pure ice state was adopted as an initial condition, and, as a consequence, the desalination of mushy ice was not involved.

In this work, we investigate the complete evolution of mushy ice in salty water within a vertical convection system using experiments and modeling. Our findings reveal that ice desalination, driven primarily by salt diffusion and only to a minor extent by brine convection within the mushy ice, controls the aging process in the experimental system. This is also reflected by the decrease in the ice porosity. To quantify this mechanism, we adopt an integral desalination model that captures well the experimental measurements. Furthermore, we observe that the system eventually reaches a state similar to that of the solidification of a pure substance in the same configuration. This work provides new measurements and insights to model brine drainage and sea ice aging.

*Contact author: fengwang2023@tsinghua.edu.cn

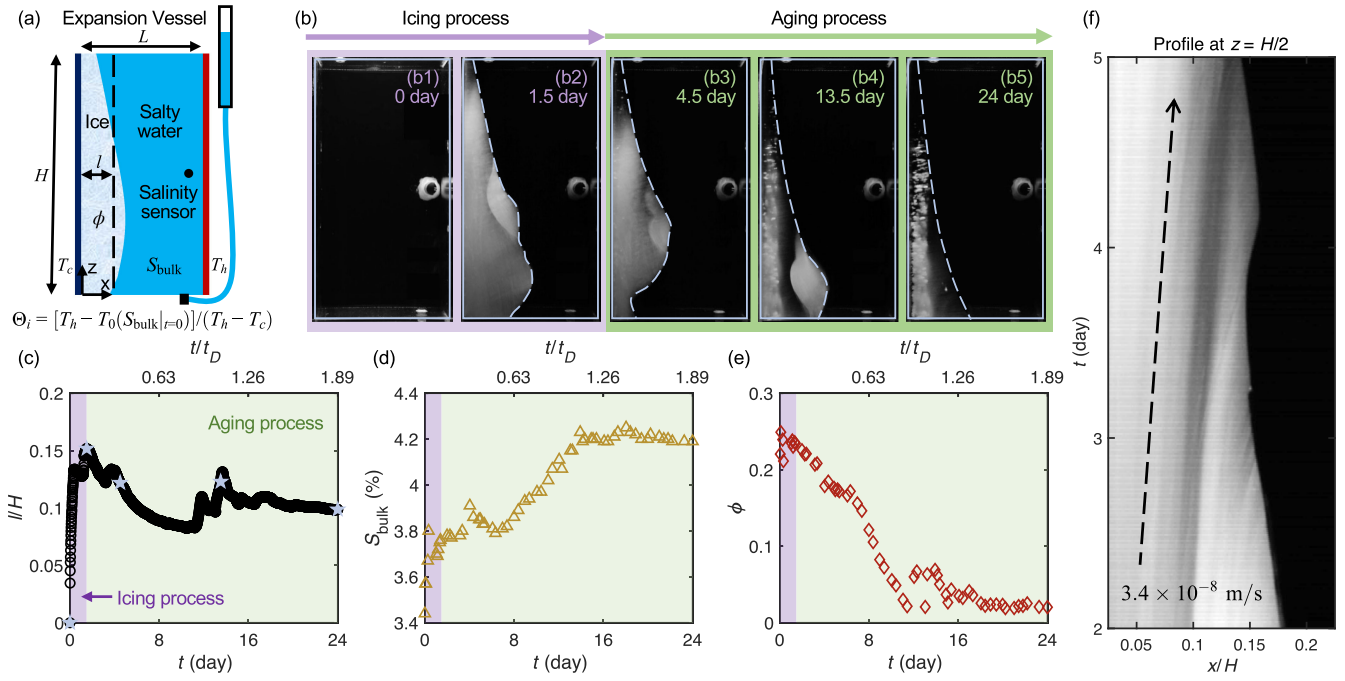

FIG. 1. Experiment on mushy ice evolution. (a) Sketch of the experimental setup. In the experiment, an ice layer, characterized by its mean thickness l and mean porosity ϕ, forms and evolves in salty water within a vertical convection system. The temperatures of the left cold plate and right hot plate are T_c and T_h. A salinity sensor measures the bulk salinity S_{bulk}. The initial superheat parameter is defined as $\Theta_i = [T_h - T_0(S_{\mathrm{bulk}}|_{t=0})]/(T_h - T_c)$, where T_0 is the freezing point at the given salinity. (b)–(f) Mushy ice evolution with $S_{\mathrm{bulk}}|_{t=0} = 3.44\%$, $T_c = -12.1\,^{\circ}\mathrm{C}$, and $T_h = 7.9\,^{\circ}\mathrm{C}$ ($\Theta_i \approx 1/2$). The ice layer undergoes first a fast icing process [(b1), (b2), and purple regime in (c)–(e)], followed by a slow aging process [(b3)–(b5) and green regime in (c)–(e)]. (b) Snapshots of the ice layer correspond to the blue stars in (c). (c)–(e) Temporal evolution of the spatially averaged ice layer thickness l made dimensionless by the system height H [black circles in (c)], bulk salinity S_{bulk} [yellow triangles in (d)], and the spatially averaged ice layer porosity ϕ [red diamonds in (e)]. The top axes show time nondimensionalized by the solutal diffusion timescale $t_D = l^{*2}/D \approx 1.1 \times 10^6$ s ≈ 12.7 days, where l^* is the mean ice thickness in the aging process and D is the salt diffusivity in the brine. (f) Space-time diagram for the ice layer profile along $z = 0.5H$ from day 2 to day 5. The internal structures of the mushy ice appear to migrate with a typical velocity of 3.0 mm/day.

Experimental setup—The experiments are performed in a quasi-two-dimensional vertical convection system [22,39–41] [Fig. 1(a)] with height $H = 0.24$ m in the z direction, length $L = 0.12$ m in the x direction, and width $W = 0.06$ m. The temperatures of the left cold plate (T_c) and right hot plate (T_h) are maintained constant. The system is initially filled with aqueous sodium chloride (NaCl) solution. In the experiments, the bulk salinity S_{bulk} is measured with a sensor, and the ice front is photographed to determine the spatially averaged ice thickness in the x direction, l. The spatially averaged ice porosity ϕ is calculated from conservation of salt, similar to [29]. To quantify the effect of temperature, an initial superheat parameter is defined as $\Theta_i = [T_h - T_0(S_{\mathrm{bulk}}|_{t=0})]/(T_h - T_c)$, where T_0 denotes the freezing point (see Supplemental Material [42] for details).

Measurement results—Figures 1(b)–1(f) display the ice layer evolution in a typical case with $S_{\mathrm{bulk}}|_{t=0} = 3.44\%$ and $\Theta_i \approx 1/2$ (see Movie S1, Movie S2, and Supplemental Material [42] for more information). The system first experiences a fast icing process at the left cold plate (purple regime in Fig. 1). The ice layer grows in about 1.5 days to a maximal thickness [Figs. 1(b1), 1(b2), and 1(c)]. As water freezes into ice, salt is not dissolvable in it. Part of the salt is expelled into the salty water reservoir external to the ice layer, increasing the bulk salinity [Fig. 1(d)]. The rest remains trapped in brine pockets in the ice matrix, leading to a highly porous ice layer [Fig. 1(e)] with a porosity roughly equivalent to that reported in previous studies [29,35,48,49]. The rapid growth of mushy ice is driven by heat transfer across the ice and is controlled by the strength of the convection in bulk salty water [21]. As the heat transfer on either side of the ice front balances [35], the rapid growth of the ice ceases.

Unlike in the freezing of fresh water or other pure liquids, the evolution of ice does not end here. Without any change in the experimental conditions, the ice layer spontaneously enters an aging process (green regime in Fig. 1), which lasts until the system converges to the final equilibrium state (about 2–3 weeks in the present case). Local advancements and retreats of the ice front occur [Figs. 1(b3)–1(b5)]; however, the average ice thickness varies with time only gradually and with an overall weak decreasing trend [Fig. 1(c)]. In contrast, the salinity of the

bulk salty water increases [Fig. 1(d)]. The average ice porosity exhibits a slow yet noticeable decline [Fig. 1(e)], and the ice layer becomes gradually transparent, as is the case for pure ice [Figs. 1(b3)–1(b5)].

Interestingly, the internal pore structures of the mushy ice appear to evolve and migrate toward the ice front over time (see Movie S1 [42]). Near the midheight of the ice layer, such migration is relatively obvious and essentially in the $+x$ direction during day 2 to day 5 (see Movie S3 [42] for an enlarged clip). Figure 1(f) shows how the photographed ice profile along $z = 0.5H$ varies over time. From this space-time diagram, a typical migration velocity can be identified to be about 3.0 mm/day.

Dynamics of ice aging—The small variation in the average ice thickness suggests that the global thermal balance of the ice layer is preserved throughout the aging process. Since it is not driven by thermal factors, what mechanism is responsible for the observed aging of mushy ice?

As heat diffusion is much faster than mass diffusion in salty water, mushy ice is in local thermal equilibrium [16] during the aging process. Figures 2(a) and 2(b) show the conceptual schematics of this process. The local temperature always equals the local freezing and melting point. The increase in temperature in the $+x$ direction (gray line) leads to a decrease in local salinity (yellow line). With such a salinity gradient, the salt is expelled from the mushy ice. The salinity of the bulk salty water increases. Meanwhile, excess water freezes inside the mushy ice, maintaining local salinity and resulting in the shrinkage of porosity.

As salt mass transfer controls the aging of ice, the characteristic timescale for this process is the solute diffusion timescale $t_D = l^{*2}/D$, where l^* labels the spatiotemporally averaged ice thickness during the desalination process and D is the salt diffusivity in the brine. For the case with $\Theta_i \approx 1/2$, t_D is about 1.1×10^6 s ≈ 12.7 days. As mentioned above, mass diffusion is much slower than heat diffusion. In fact, the Lewis number $\mathrm{Le} = \kappa/D$ is roughly 200, where κ is the brine thermal diffusivity. This explains the significant difference between the timescales of the icing process and the aging process [see Figs. 1(c)–1(e)].

The apparent velocity scale for salt diffusion can be estimated by dividing the diffusive salt flux $D(S_c - S_{\mathrm{bulk}})/l$ with the reference salinity $(S_c + S_{\mathrm{bulk}})/2$, i.e., $v_D = 2D(S_c - S_{\mathrm{bulk}})/[l(S_c + S_{\mathrm{bulk}})]$ [13,50], where S_c is the salinity at the cold plate determined by its temperature T_c and the bulk salinity S_{bulk} is approximately the salinity at the ice front, assuming sufficiently strong convective mixing in the bulk. Considering the pore structures inside the mushy ice [Fig. 2(b)], the saltier (colder) side freezes while the fresher (hotter) side melts with the diffusion of salt. Therefore, the apparent velocity scale for salt diffusion also reflects the typical migration velocity of internal pore structures [51]. For the case in Fig. 1(f), it is about 1.8–2.3 mm/day, close to the observed migration velocity. The remaining difference might come from the influence of

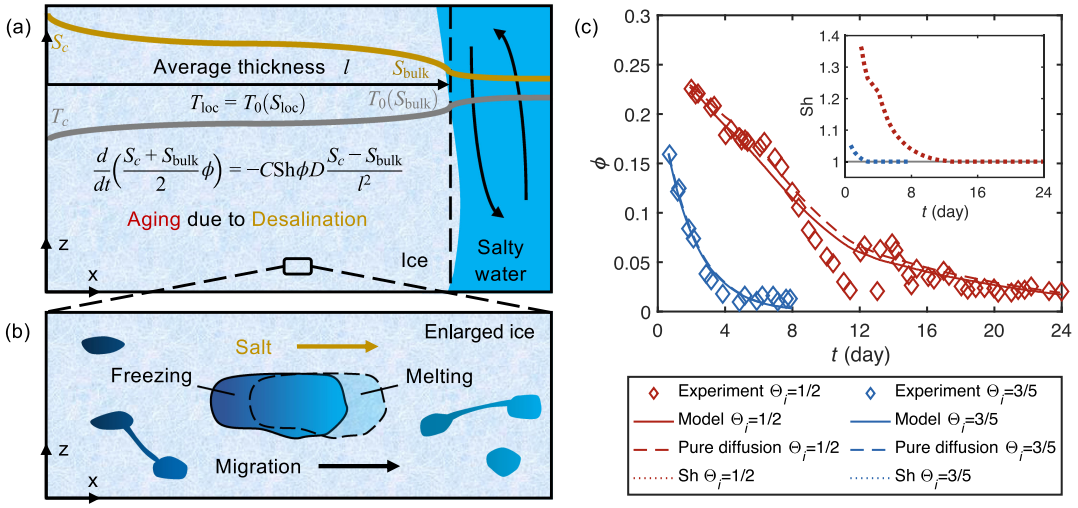

FIG. 2. Dynamics for mushy ice aging in salty water. (a),(b) Conceptual schematic of the desalination and aging of mushy ice for illustrative purposes. (a) Sketch of the desalination of the whole ice layer. The reduction of salt in the mushy ice equals salt removed through diffusion and advection. The gray line sketches the variation of local temperature in the x direction, while the yellow line represents local salinity. The local temperature and salinity are related by the local thermal equilibrium in the mushy ice. (b) Enlarged sketch of the migration of pores inside the mushy ice. With the transport of salt, the colder (saltier) side freezes while the hotter (fresher) side melts, leading to the migration of ice internal structures. (c) Integral desalination model (solid lines) and experiment (diamonds) results for the evolution of spatially averaged ice layer porosity ϕ, with initial superheat parameters $\Theta_i \approx 1/2$ (red) and 3/5 (blue). The model predictions when advective transport is neglected by imposing $\mathrm{Sh} \equiv 1$ (dashed lines) are also attached for comparing the relative role of diffusion and advection. For $\Theta_i \approx 3/5$, the blue dashed line overlaps largely with the blue solid line. The inset in (c) shows the corresponding time evolution of Sh from the model (dotted lines).

nonuniform ice thickness and porosity on the global and local desalination characteristics, as well as the influence of brine convection.

Noteworthily, the decrease in the global salt content in the mushy layer is directly related to the salt released into the bulk salty water as the pores migrate to the ice front, as the result of an effective diffusive process controlled by the evolving salinity gap across the also evolving ice layer [see Fig. 2(a)]. The temporal evolution of this process can be captured by the following integral desalination model:

$$\frac{d}{dt}\left(\frac{S_c + S_{\mathrm{bulk}}}{2}\phi\right) = -C\,\mathrm{Sh} v_D\,\phi\frac{S_c + S_{\mathrm{bulk}}}{2l} = -C\,\mathrm{Sh}\phi D\,\frac{S_c - S_{\mathrm{bulk}}}{l^2}, \quad (1)$$

where S_c is the salinity at the cold plate determined by T_c in the experiment; S_{bulk} is the bulk salty water salinity and l is the average ice thickness, both extracted from experiments; D is the salt diffusivity; Sh is the Sherwood number representing the dimensionless mass transfer efficiency due to convection in mushy ice, whose estimation is shown in End Matter; parameter C compensates for influences of nonuniform ice thickness and porosity (see details in Supplemental Material [42]). With a given initial value of porosity ϕ, the temporal evolution of ϕ can be explicitly solved by the model.

We choose $C = 1.1$ for $\Theta_i \approx 1/2$ (red) and $C = 2.2$ for $\Theta_i \approx 3/5$ (blue) to best fit the experimental data. Figure 2(c) compares the model (lines) and experimental (diamonds) results for the average porosity ϕ over time. The model agrees well with the experimental results, demonstrating that it effectively captures the desalination mechanism that governs the aging dynamics of the ice. Convective salt transport inside the ice occurs only at the beginning of the process and plays a much more limited role in the desalination and ice aging within the parameter regime of the current system. This is evident from the inset in Fig. 2(c) and also from the small differences between the solid lines (including advective transport) and the dashed lines (assuming pure diffusion) in Fig. 2(c), main panel, which is even negligible when $\Theta_i \approx 3/5$ (blue). This result explains why the duration of the aging process and the migration velocity of the observed patterns are comparable to the timescale and the velocity scale of salt diffusion, as shown in Figs. 1(c)–1(e) and discussed above. A weakening convection in mushy ice when $\Theta_i \approx 1/2$ also explains the overall decrease in ice thickness through the aging process, whereas the negligible convection in mushy ice explains the very small changes in ice thickness for $\Theta_i \approx 3/5$ [35].

Naturally, the local formation and melting of more porous or less porous regions within the ice layer influence the average porosity. A detailed explanation of the ice morphology evolution is highly challenging, as it requires detailed and nonintrusive measurements of the velocity, temperature, and salinity fields in the mushy ice and in the bulk salty water. Still, it is worth pointing out that the final form of the ice front (yellow dashed line in Fig. 3) overlaps remarkably well with the one obtained from direct numerical simulations of the solidification of a pure liquid (thin black line in Fig. 3). In the simulations, we use the same physical properties (same salinity and same freezing point) for the fluid as those of the salty water in the final state of the experiment. The results suggest that the final ice layer in the experiment is, in practice, a pure ice layer, and the bulk salty water eventually becomes well mixed with uniform salinity. Vertical convective flow dominates in the final bulk salty water, with temperature imbalances being the sole contributor to density differences and buoyancy. We refer to Supplemental Material [42] for more details.

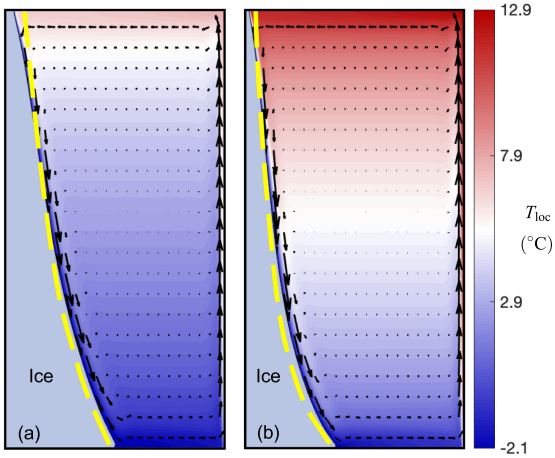

FIG. 3. Asymptotic equilibrium state of the system. The final ice front morphologies from the experiment (yellow dashed line) are compared with those from direct numerical simulation of a positively buoyant pure liquid freezing under the same conditions (thin black line). The color shows the temperature field in the liquid phase, while the small black arrows indicate the velocity field, both from the simulation. The "*ad hoc*" positively buoyant liquid possess the same thermal properties as salty water with the bulk salinity measured at the end of the experiments. (a) $\Theta_i \approx 1/2$. (b) $\Theta_i \approx 3/5$.

Overall, the combined experimental, theoretical, and numerical results provide a consistent understanding of the dynamics of ice aging in salty water. They highlight the critical role of thermal gradients in salinity and ice porosity evolution and the eventual transformation of mushy ice into solid ice.

Conclusion and outlook—In summary, we study the complete evolution of ice in salty water in a vertical convective flow system, with a focus on the dynamics of its spontaneous aging. We show that, in the present system and parameter regime, the observed aging of mushy ice is driven primarily by diffusive desalination and to a minor extent by convective desalination. The long-term decline of ice porosity can be well predicted using an integral model that quantifies the salt flux out of the ice layer. In addition,

we find that the final state of the system, consisting of a dense ice layer and a well-mixed salty water zone, is highly consistent with the freezing of a positively buoyant pure liquid under the same conditions.

Our results advance the understanding of the coupled dynamics of fluid flow, mass and heat transfer, and phase change in aqueous solution systems. In natural scenarios of sea ice, rapid freezing and melting are dominating in the case of drastic thermal disequilibrium, while diffusion-driven desalination and aging of sea ice are slow and occur in the long term. This indicates the need to adopt a multilayer model for multiyear sea ice, as it may experience multiple freezings and meltings during its aging. Noteworthily, there can also exist stronger desalination processes such as flushing or brine convection, accelerating the aging of sea ice. Although the aging of real-world sea ice is more complex, our findings provide a valuable example of how this process can be investigated and parametrized through laboratory studies. Future work could explore different flow geometries and incorporate the effects of multicomponent salts and impurities typically found in natural seawater. It would also be important to investigate how the aging process affects the overall heat transfer in ice and bulk salty water. Combining field measurements with laboratory studies will provide new insights into the natural aging of sea ice, refine parametrizations, and enable more accurate integration into climate models, helping bridge the gap between controlled experiments and the complexities of sea ice dynamics in natural environments.

Acknowledgments—We thank Rui Yang for insightful discussions. This work is supported by National Natural Science Foundation of China Excellence Research Group Program for "Multiscale Problems in Nonlinear Mechanics" (No. 12588201), the National Natural Science Foundation of China under Grant No. 12402321, the New Cornerstone Science Foundation through the New Cornerstone Investigator Program and the XPLORER PRIZE, and Shuimu Tsinghua Scholar Program under Grant No. 2023SM038.

Data availability—The data that support the findings of this Letter are openly available [52].

[1] Y. Du, E. Calzavarini, and C. Sun, Nat. Rev. Phys. **6**, 676 (2024).
[2] G. W. Timco and W. F. Weeks, Cold Reg. Sci. Technol. **60**, 107 (2010).
[3] D. Feltham, Annu. Rev. Fluid Mech. **40**, 91 (2008).
[4] C. Cenedese and F. Straneo, Annu. Rev. Fluid Mech. **55**, 377 (2023).
[5] L. A. Roach, M. M. Smith, A. Herman, and D. Ringeisen, Annu. Rev. Mar. Sci. **17**, 355 (2024).
[6] J. Maslanik, J. Stroeve, C. Fowler, and W. Emery, Geophys. Res. Lett. **38**, L13502 (2011).
[7] A. A. Korosov, P. Rampal, L. T. Pedersen, R. Saldo, Y. Ye, G. Heygster, T. Lavergne, S. Aaboe, and F. Girard-Ardhuin, Cryosphere **12**, 2073 (2018).
[8] M. Mori, Y. Kosaka, M. Watanabe, H. Nakamura, and M. Kimoto, Nat. Clim. Change **9**, 123 (2019).
[9] J. A. Screen and I. Simmonds, Nature (London) **464**, 1334 (2010).
[10] I. Peeken, S. Primpke, B. Beyer, J. Gütermann, C. Katlein, T. Krumpen, M. Bergmann, L. Hehemann, and G. Gerdts, Nat. Commun. **9**, 1505 (2018).
[11] E. Post, U. S. Bhatt, C. M. Bitz, J. F. Brodie, T. L. Fulton, M. Hebblewhite, J. Kerby, S. J. Kutz, I. Stirling, and D. A. Walker, Science **341**, 519 (2013).
[12] K. R. Arrigo, Annu. Rev. Mar. Sci. **6**, 439 (2014).
[13] D. Notz and M. G. Worster, J. Geophys. Res. Oceans **114**, C05006 (2009).
[14] E. C. Hunke, D. Notz, A. K. Turner, and M. Vancoppenolle, Cryosphere **5**, 989 (2011).
[15] F. P. Jardon, F. Vivier, M. Vancoppenolle, A. Lourenço, P. Bouruet-Aubertot, and Y. Cuypers, J. Geophys. Res. Oceans **118**, 435 (2013).
[16] D. L. Feltham, N. Untersteiner, J. S. Wettlaufer, and M. G. Worster, Geophys. Res. Lett. **33**, L14501 (2006).
[17] M. G. Worster and D. W. Rees Jones, Phil. Trans. R. Soc. A **373**, 20140166 (2015).
[18] D. M. Anderson and P. Guba, Annu. Rev. Fluid Mech. **52**, 93 (2020).
[19] B. Rabbanipour Esfahani, S. C. Hirata, S. Berti, and E. Calzavarini, Phys. Rev. Fluids **3**, 053501 (2018).
[20] R. Yang, C. J. Howland, H. R. Liu, R. Verzicco, and D. Lohse, PRX Energy **3**, 043006 (2024).
[21] Z. Wang, E. Calzavarini, C. Sun, and F. Toschi, Proc. Natl. Acad. Sci. U.S.A. **118**, e2012870118 (2021).
[22] Z. Wang, L. Jiang, Y. Du, C. Sun, and E. Calzavarini, Phys. Rev. Fluids **6**, L091501 (2021).
[23] Z. Wang, E. Calzavarini, and C. Sun, Europhys. Lett. **135**, 54001 (2021).
[24] S. Weady, J. Tong, A. Zidovska, and L. Ristroph, Phys. Rev. Lett. **128**, 044502 (2022).
[25] D. Perissutti, C. Marchioli, and A. Soldati, Int. J. Multiphase Flow **181**, 105007 (2024).
[26] R. Yang, C. J. Howland, H. R. Liu, R. Verzicco, and D. Lohse, Phys. Rev. Lett. **131**, 234002 (2023).
[27] M. E. Wengrove, E. C. Pettit, J. D. Nash, R. H. Jackson, and E. D. Skyllingstad, Nat. Geosci. **16**, 871 (2023).
[28] W. P. Fang, J. Z. Wu, Z. L. Huang, B. F. Wang, Q. Zhou, and K. L. Chong, J. Fluid Mech. **1001**, A43 (2024).
[29] J. S. Wettlaufer, M. G. Worster, and H. E. Huppert, J. Fluid Mech. **344**, 291 (1997).
[30] M. G. Worster, Annu. Rev. Fluid Mech. **29**, 91 (1997).
[31] S. S. L. Peppin, P. Aussillous, H. E. Huppert, and M. G. Worster, J. Fluid Mech. **570**, 69 (2007).
[32] S. S. L. Peppin, H. E. Huppert, and M. G. Worster, J. Fluid Mech. **599**, 465 (2008).
[33] C. A. Middleton, C. Thomas, A. De Wit, and J. L. Tison, J. Glaciol. **62**, 1 (2016).
[34] A. J. Wells, J. R. Hitchen, and J. R. G. Parkinson, Phil. Trans. R. Soc. A **377**, 20180165 (2019).
[35] Y. Du, Z. Wang, L. Jiang, E. Calzavarini, and C. Sun, J. Fluid Mech. **960**, A35 (2023).

[36] M. Mondal, B. Gayen, R. W. Griffiths, and R. C. Kerr, J. Fluid Mech. **863**, 545 (2019).
[37] N. J. Wilson, C. A. Vreugdenhil, B. Gayen, and E. W. Hester, Geophys. Res. Lett. **50**, e2023GL104396 (2023).
[38] R. Yang, C. J. Howland, H. R. Liu, R. Verzicco, and D. Lohse, J. Fluid Mech. **969**, R2 (2023).
[39] C. S. Ng, A. Ooi, D. Lohse, and D. Chung, J. Fluid Mech. **764**, 349 (2015).
[40] O. Shishkina, Phys. Rev. E **93**, 051102(R) (2016).
[41] C. J. Howland, R. Verzicco, and D. Lohse, Phys. Rev. Fluids **8**, 013501 (2023).
[42] See Supplemental Material at http://link.aps.org/supplemental/10.1103/mct1-6hbw, which includes Refs. [43–47], for the additional details of experimental setup and data measurements, experiment results for $\Theta_i \approx 3/5$, choice of C in the model, numerical simulation, flow chart on the measurement and modeling of porosity, and supplemental movies.
[43] E. Calzavarini, Soft. Impacts **1**, 100002 (2019).
[44] L. Jiang, C. Sun, and E. Calzavarini, Phys. Rev. E **99**, 013108 (2019).
[45] S. C. Gupta, *The Classical Stefan Problem Basic Concepts, Modelling and Analysis with Quasi-Analytical Solutions and Methods* (Elsevier, New York, 2017).
[46] B. Gebhart and J. C. Mollendorf, Deep Sea Res. **24**, 831 (1977).
[47] D. L. Hall, S. M. Sterner, and R. J. Bodnar, Econ. Geol. **83**, 197 (1988).
[48] C. Petrich, P. J. Langhorne, and Z. F. Sun, Cold Reg. Sci. Technol. **44**, 131 (2006).
[49] M. G. Worster and J. S. Wettlaufer, J. Phys. Chem. B **101**, 6132 (1997).
[50] A. W. Rempel, E. D. Waddington, J. S. Wettlaufer, and M. G. Worster, Nature (London) **411**, 568 (2001).
[51] P. Hoekstra, T. E. Osterkamp, and W. F. Weeks, J. Geophys. Res. **70**, 5035 (1965).
[52] Y. Du, F. Wang, E. Calzavarini, and C. Sun, 10.5281/zenodo.15781015.
[53] A. Bejan and K. R. Khair, Int. J. Heat Mass Transfer **28**, 909 (1985).
[54] K. J. Schneider, in *Proceedings of the 11th International Congress of Refrigeration* (1963), Vol. 247, p. 253.

End Matter

Derivation of the integral model—Neglecting salt dissolution in ice and the density difference between brine and ice, the governing equation for the local salt conservation in the porous ice reads [13,16]

$$\partial(S_{\mathrm{loc}}\phi_{\mathrm{loc}})/\partial t = \nabla\cdot(\phi_{\mathrm{loc}}D\nabla S_{\mathrm{loc}}) - \phi_{\mathrm{loc}}\mathbf{u}\cdot\nabla S_{\mathrm{loc}}, \quad \text{(A1)}$$

where S_{loc} is the local salinity in the brine, ϕ_{loc} is the local porosity, D is the salt diffusivity, and $\mathbf{u}$ is the brine velocity. While solving Eq. (A1) directly is complex, its physical interpretation is straightforward: The rate of change for the mass of salt is determined by the diffusive and advective transport of salt.

We estimate the rate of change for the total mass of salt in ice as

$$\frac{d}{dt}\left(\frac{S_c + S_{\mathrm{bulk}}}{2}\phi\right)\rho_m lHW, \quad \text{(A2)}$$

where $(S_c + S_{\mathrm{bulk}})/2$ is approximately the average salinity of the brine in the mushy ice and $\phi\rho_m lHW$ is the mass of brine in the mushy ice. Here, we neglect the time dependence of ρ_m and l, since their variations are small.

Assuming that S_{bulk} is roughly the salinity at the ice front, the diffusive and advective transport of salt from ice into bulk salty water are estimated jointly as

$$C\,\mathrm{Sh}\phi D\,\frac{S_c - S_{\mathrm{bulk}}}{l}\,\rho_m HW, \quad \text{(A3)}$$

where parameter C is introduced to compensate for the nonuniform ice thickness and porosity. The Sherwood number $\mathrm{Sh} = Jl/[D(S_c - S_{\mathrm{bulk}})]$ quantifies the dimensionless mass transport efficiency due to convection (sum of diffusion and advection), where J is the salt flux.

Finally, by equating Eqs. (A2) and (A3), we obtain the integral model [Eq. (1)].

Estimation of the Sherwood number—The convection in mushy ice in our study is mainly driven by salinity gradient. The scaling of mass transfer is comparable to that of heat transfer for convection driven by temperature gradient [53]. We obtain the estimation for Sh by fitting the experimental data in [54]:

$$\mathrm{Sh} = 1 + 0.04\,(l/H)^2\mathrm{LeRa}. \quad \text{(B1)}$$

Le is the Lewis number, representing the ratio of thermal diffusivity κ to the mass diffusivity of salt D:

$$\mathrm{Le} = \kappa/D. \quad \text{(B2)}$$

Ra is the Rayleigh number, which parametrizes the relative role of the buoyancy intensity driving the convection with respect to the thermal and kinetic dissipation:

$$\mathrm{Ra} = \frac{KgH}{\kappa\nu}\,\frac{\rho_c - \rho_0}{\rho_0}, \quad \text{(B3)}$$

where g is gravitational acceleration, H is the system height, ν is the kinetic viscosity, ρ_c is the brine density at the cold plate, and ρ_0 is the brine density at the ice front.

The permeability K (unit m^2) in the definition of Ra depends on the structure of the ice. It is estimated as a function of the average ice porosity ϕ, modified from the empirical equation in a previous study [48]:

$$K = \begin{cases} 0, & \phi < 0.054, \\ 2 \times 10^{-11}(\phi - 0.054)^{1.2}, & \phi > 0.054. \end{cases} \tag{B4}$$

This estimate is in good agreement with previous laboratory and field results [48].

Table of symbols—A summary of the symbols and their physical meanings are provided in Table I, for convenience of reading.

TABLE I. Summary of symbols and their physical meanings.

Symbol	Physical meaning
C	Correcting coefficient
D	Diffusivity of salt in brine
g	Gravitational acceleration
H	Height of experiment system
J	Salt flux
K	Permeability
L	Length of experiment system
l	Spatially averaged ice layer thickness
l^*	Mean ice thickness in aging process
Le	Lewis number
Ra	Rayleigh number in mushy ice
S_{bulk}	Salinity of bulk salty water
S_c	Salinity at the cold plate
S_{loc}	Local salinity
Sh	Sherwood number
T_c	Left cold plate temperature
T_h	Right hot plate temperature
$T_0(S)$	Freezing and melting point at salinity S
t	Time
t_D	Solutal diffusion time scale
$\mathbf{u}$	Local velocity in brine in mushy ice
v_D	Apparent velocity scale of salt diffusion
W	Width of experiment system
κ	Brine thermal diffusivity
ν	Brine kinetic viscosity
ϕ	Spatially averaged ice layer porosity
ϕ_{loc}	Local ice porosity
ρ_0	Salty water density at ice front
ρ_c	Brine density at the cold plate
ρ_m	Brine density in the mushy ice
Θ_i	Initial hot plate superheat parameter